

See discussions, stats, and author profiles for this publication at: <https://www.researchgate.net/publication/233913146>

3-Dimensional Graphene Carbon Nanotube Carpet-Based Microsupercapacitors with High Electrochemical Performance

ARTICLE *in* NANO LETTERS · DECEMBER 2012

Impact Factor: 13.59 · DOI: 10.1021/nl3034976 · Source: PubMed

CITATIONS

126

READS

293

8 AUTHORS, INCLUDING:



Jian Lin

University of Missouri

42 PUBLICATIONS 995 CITATIONS

[SEE PROFILE](#)



Zheng Yan

University of Illinois, Urbana-Champaign

35 PUBLICATIONS 2,145 CITATIONS

[SEE PROFILE](#)



Zhiwei Peng

University of Maryland, College Park

49 PUBLICATIONS 1,483 CITATIONS

[SEE PROFILE](#)



Douglas Natelson

Rice University

194 PUBLICATIONS 4,595 CITATIONS

[SEE PROFILE](#)

3-Dimensional Graphene Carbon Nanotube Carpet-Based Microsupercapacitors with High Electrochemical Performance

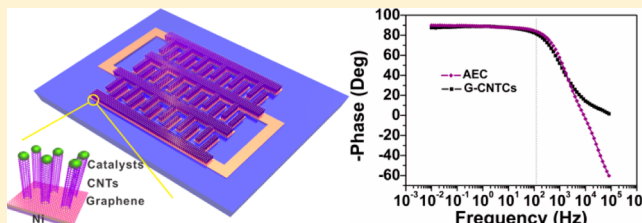
Jian Lin,^{†,‡} Chenguang Zhang,^{‡,§,⊥} Zheng Yan,[§] Yu Zhu,^{‡,§} Zhiwei Peng,[§] Robert H. Hauge,^{‡,§} Douglas Natelson,^{*,||,‡} and James M. Tour^{*,†,‡,§,▽}

[†]Department of Mechanical Engineering and Material Science, [‡]Smalley Institute for Nanoscale Sci. & Tech, [§]Department of Chemistry, ^{||}Department of Physics and Astronomy, [#]Department of Electrical and Computer Engineering, and [▽]Department of Computer Science, Rice University, 6100 Main St., Houston, Texas 77005, United States

[⊥]School of Materials Science and Engineering, Tianjin University, Tianjin 300072, China

Supporting Information

ABSTRACT: In this research, 3-dimensional (3D) graphene/carbon nanotube carpets (G/CNTCs)-based microsupercapacitors (G/CNTCs-MCs) were fabricated *in situ* on nickel electrodes. The G/CNTCs-MCs show impedance phase angle of -81.5° at a frequency of 120 Hz, comparable to commercial aluminum electrolytic capacitors (AECs) for alternating current (ac) line filtering applications. In addition, G/CNTCs-MCs deliver a high volumetric energy density of 2.42 mWh/cm^3 in the ionic liquid, more than 2 orders of magnitude higher than that of AECs. The ultrahigh rate capability of 400 V/s enables the microdevices to demonstrate a maximum power density of 115 W/cm^3 in aqueous electrolyte. The high-performance electrochemical properties of G/CNTCs-MCs can provide more compact ac filtering units and discrete power sources in future electronic devices. These elevated electrical features are likely enabled by the seamless nanotube/graphene junctions at the interface of the differing carbon allotropic forms.



KEYWORDS: 3-Dimensional, microsupercapacitors, graphene, carbon nanotube carpets

Increasing demand for portable electronics and miniaturized wireless sensor networks has spawned great interest among materials scientists in their quest for compatible energy storage devices.^{1–6} The microsupercapacitor has gained special attention due to the possibility of integration as discrete power sources for microelectromechanical systems (MEMS).^{7–11} Recently, great advancements in improving the power/energy density or rate capability of microsupercapacitors have been achieved through exploring a variety of materials such as carbide-derived carbon (CDC),⁷ onion-like carbon (OLC),⁸ laser reduced/scribed graphene,^{9,11} activated carbon (AC),¹⁰ and metal oxide/carbon composites.^{12,13} However, the investigation of materials for supercapacitors with capabilities compatible with 120 Hz alternating current (ac)-line filtering performance is still in its infancy.^{14,15}

120 Hz ac line filtering is the function that smoothes the leftover ac ripple on direct current (dc) voltage buses in power-line supply electronics.¹⁴ The full-wave rectified 60 Hz ac power is then filtered to produce the pure dc voltage.¹⁴ It is especially important in the renewable electrical power generated by wind or hydroelectric turbines in which frequency variance can be caused because of uncontrollable wind or water flow. Filtering efficacy is usually characterized by the impedance phase angle (a “factor of merit”¹⁵) when the input frequency is 120 Hz. Currently, aluminum electrolytic capacitors (AECs) are widely used for this purpose, though AECs suffer from low

energy density. Supercapacitors, also called electrical double-layer capacitors (DLC), can deliver much higher energy densities. However, due to the slow, lossy internal response of the polarization, the phase angle for commercial supercapacitors at 120 Hz is close to 0° , not applicable in ac line filtering. There is great interest in achieving high energy density while maintaining a satisfactory ac response in a single device. In this way, supercapacitors with ac line filtering performance will reduce the system size and weight in portable electronics.^{14,15} In attempts to improve the ac frequency response, vertically aligned carbon nanotubes (VA-CNTs) have been explored as electrode materials for supercapacitors. Prior efforts did not yield the desired ac response because of a high interfacial resistance between VA-CNTs and the current collector, either caused by an insulating buffer layer^{12,16} or the transfer procedure^{13,17} used to place the tubes. Therefore, the *in situ* synthesis of CNTs directly on a highly conductive medium with a good electrical connection is desired to produce supercapacitors with ac-line filtering performances. Recent advancement in the synthesis of carbon nanotube carpets (CNTCs) grown seamlessly from graphene to form the 3-

Received: September 19, 2012

Revised: November 26, 2012

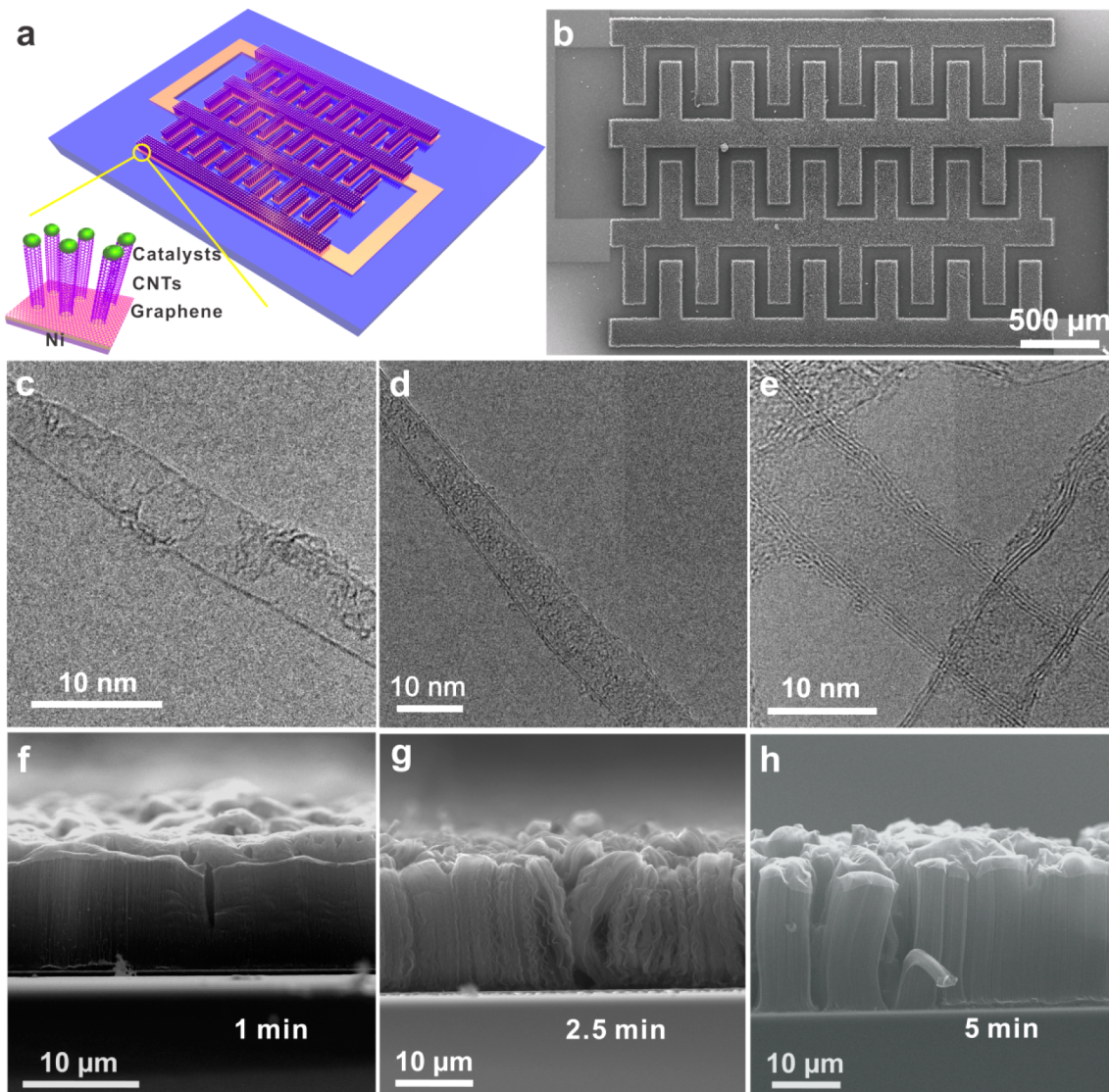


Figure 1. Design of microsupercapacitors and material characterizations of CNTCs. (a) Schematic of the structure of G/CNTCs-MCs. Inset: enlarged scheme of Ni-G-CNTCs pillar structure that does not show the Al_2O_3 atop the CNTCs; (b) SEM image of a fabricated G/CNTCs-MC; (c–e) TEM images of individual single-, double-, and few-wall CNTs; (f–h) cross-sectioned SEM images of CNTCs grown for 1, 2.5, and 5 min.

dimensional (3D) hybrid material provides a possible route.^{18–20}

Here we show that graphene/CNTCs (G/CNTCs) can provide the desired electrochemical characteristics. We report the fabrication of microsupercapacitors based on 3D G/CNTCs with seamlessly patterned CNTCs grown from the graphene. The 3D G/CNTCs hybrid materials are directly and intimately connected to nickel current collectors, providing good interfacial electrical conduction. The as-fabricated micro-devices show an impedance phase angle as large as -81.5° at a frequency of 120 Hz, comparable to that seen in AECs. At the same time, the new devices offer specific capacitances up to 2.16 mF/cm^2 in aqueous electrolytes and 3.93 mF/cm^2 in ionic liquids, comparable with some of the best reported results in all supercapacitors. The measured discharge rate, up to 400 V/s, is hundreds of times higher than that shown in most supercapacitors, enabling the devices to deliver a theoretical maximum power density of 115 W/cm^3 even in aqueous electrolyte. A high energy density of 2.42 mWh/cm^3 was achieved in ionic liquids. All of these high electrochemical

performance characteristics will enable G/CNTCs-MCs to act as more compact ac filtering units and discrete power sources in future electronics.

The structure of the 3D G/CNTCs-MCs is schematically illustrated in Figure 1a. The inset is the magnified structure, showing CNTCs-graphene-Ni pillars with catalysts (iron/alumina) on the top. The microdevices were fabricated as follows. First, the interdigital-finger geometry was patterned using conventional photolithography on Si/SiO₂ substrates, followed by the deposition of Cr (10 nm) adhesion layer and Ni (450 nm) graphene growth catalyst layer. Few-layer graphene (FLG) was then grown on the patterned Ni electrodes by chemical vapor deposition (CVD).²¹ After this, catalyst particles (Fe/Al₂O₃) were patterned and deposited on the FLG. In the final step, CNTCs were synthesized on FLG by CVD. The detailed process is illustrated in the Supporting Figure S1 and described further in the Supporting Experimental Information.

Figure 1b is a representative scanning electron microscopy (SEM) image of a fabricated G/CNTCs-MC. In general, the

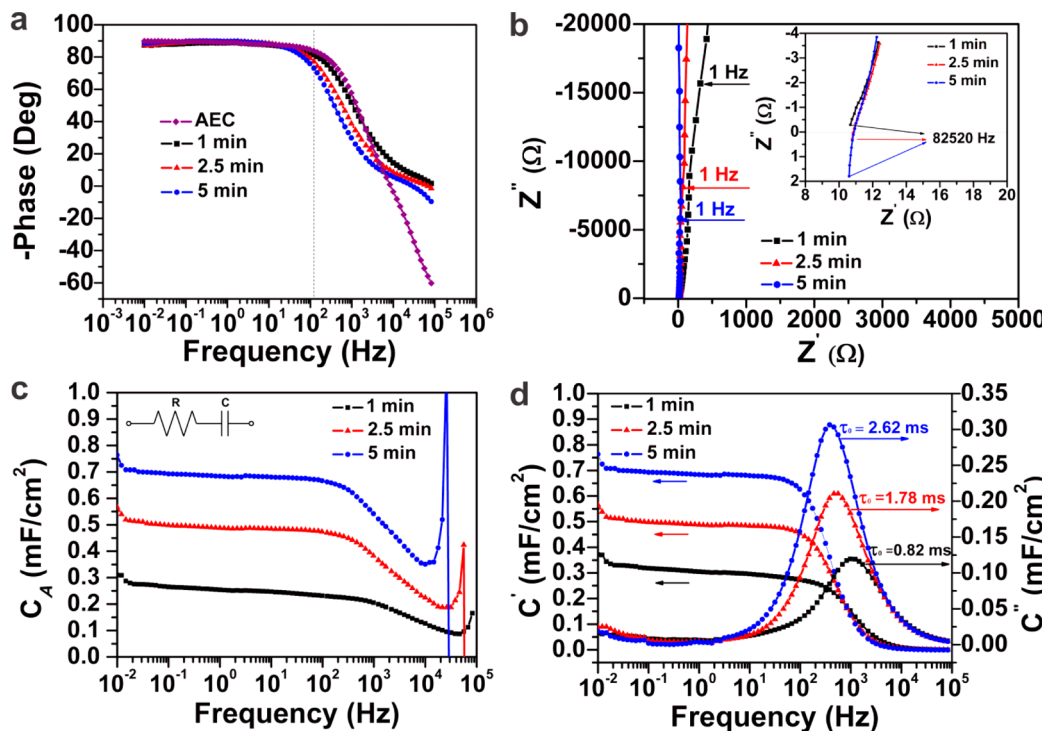


Figure 2. The ac impedance characterizations of microsupercapacitors with CNTCs grown for various durations (1, 2.5, and 5 min) using 1 M Na_2SO_4 . (a) Impedance phase angle versus frequency. The phase angles occurring at 120 Hz are 81.5° , 77.2° , and 73.4° for 1, 2.5, and 5 min growth, respectively; the phase angle at 120 Hz for an AEC is 83.9° ; (b) Nyquist plots of impedance from the three different growth-time structures. The inset is the expanded view in the high-frequency region; (c) C_A versus f using series-RC circuit model; τ_{RC} of 195, 325, and 402 μs were obtained for 1, 2.5, and 5 min growth; a Randels equivalent circuit representing the RC circuit elements is show in the inset; (d) C' and C'' versus f . The extremely low τ_0 of 0.82, 1.78, and 2.62 ms were extracted from 1, 2.5, and 5 min growth.

CNTCs are split into 1–2 μm of individual CNT pitches, whose exposed tip-ends are capped by Fe/ Al_2O_3 (Supporting Figure S2a). This nanotube tip-growth process has been called Odako growth.^{20,22} Using small, individual pitches allows the electrolyte to penetrate readily into the active CNTs, thus enhancing the specific capacitance and the frequency response. During the growth process, the role of the graphene is to prevent the iron catalysts from being alloyed with the Ni electrodes. This assumption is supported by the results of control experiments, showing that CNTCs were difficult to grow directly on the Ni electrodes without the previous coverage of graphene (Supporting Figure S2b). The Raman spectrum of as-grown FLG exhibits a low defect peak (Supporting Figure S2c), indicating reasonably high-quality growth. The characteristic Raman spectrum of as-grown CNTCs is shown in Supporting Figure S2d. The low D/G band intensity ratio (I_D/I_G) of 1:9 likewise indicates the high quality of CNTs. The clear radial breathing mode (RBM) reveals the existence of high-quality CNTs with small diameters,^{16,20} which is further depicted in the transmission electron microscopy (TEM) images (Figure 1c–e). From the TEM images we can see that most CNTs in the carpets are single-, double-, and few-walled with diameters varying from 4 to 8 nm. These dense CNTs with small diameters were reported to offer ultrahigh surface area.²⁰ To investigate the influence of the heights of the CNTCs on the electrochemical performance of microsupercapacitors, CNTCs were grown for 1, 2.5, and 5 min, affording heights of ~ 10 , 15, and 20 μm , respectively, as shown in Figure 1f–h. From the SEM images, it is evident that the CNTCs were grown vertically from the graphene surface, without any alumina buffer layer in between.

This connection provides excellent electrical conduction between the active material and the current collectors.²⁰

To evaluate the ac response of the fabricated G/CNTCs-MCs, electrochemical impedance spectroscopy (EIS) measurements were performed. The impedance phase angles of microsupercapacitors constructed with CNTCs grown for various durations (1, 2.5, and 5 min) are plotted as functions of frequency (Figure 2a). The absolute phase angles of all of the three microdevices at the low frequency region (< 50 Hz) are very close to 90° , which is indicative of near-ideal capacitive response. The absolute phase angle of the microdevice fabricated with 1 min growth CNTCs is 81.5° at 120 Hz, which is comparable to commercial AECs (83.9° , Figure 2a) and higher than hitherto reported values from CNTs ($< 75^\circ$).²³ As the growth duration increases to 5 min, the height of the CNTCs increases from ~ 10 to ~ 20 μm . This leads to a necessarily longer ion diffusion length as well as an increased electrical resistance between the tube base and tip. As a result, the absolute phase angle at 120 Hz decreases to 73.4° for the microdevice with 5 min growth CNTCs. For the ease of comparison, one often studies the frequency when the impedance phase angle reaches -45° . The frequencies (f) at a phase angle of -45° are ~ 1343 , 754, and 460 Hz for the as-fabricated microdevices with CNTCs grown for 1, 2.5, and 5 min, respectively (Figure 2a). These crossover frequencies are more than 2 orders of magnitude higher than activated carbon microsupercapacitors (AC-MCs, < 5 Hz)¹⁰ and much higher than OLC microsupercapacitors (OLC-MCs, < 100 Hz),⁸ laser-reduced graphene microsupercapacitors (LRG-MCs, < 5 Hz),⁹ or laser-scribed graphene double-layer capacitors (LSG-DLC, 30 Hz).¹¹

Table 1. Comparison of Electrochemical Performance of Various Capacitors Built in Different Materials^a

device	reference	material	phase at 120 Hz	<i>f</i> (Hz) at -45°	τ_{RC} (ms)	τ_0 (ms)	R_C (V/s)	C_A (mF/cm ²)	P_v (W/cm ³)	E_v (mWh/cm ³)
microdevice	current work	G-CNTCs	81.5°	1343	0.195	0.82	400	2.16 3.93 0.9 <i>~</i> 1000	115 135 <i>~</i> 1000 <i>~</i> 1000	0.16 2.42 <i>~</i> 1 <i>~</i> 5
	Pech et al. ⁸	OLC	N/A	<100 ^b	N/A	26	100	N/A 0.9 <i>~</i> 1000	N/A <i>~</i> 1000 <i>~</i> 1000	N/A <i>~</i> 1 <i>~</i> 5
	Gao et al. ⁹	LRG	N/A	<5 ^b	N/A	N/A	<0.1	~1.0 ~2.5	~100 ~10	<1 ~5
	Pech et al. ^{8,10}	AC	<1 ^b	<5 ^b	N/A	700	1	N/A 2.1 N/A 2.1	N/A <i>~</i> 30 <i>~</i> 30	N/A <i>~</i> 10 <i>~</i> 10
macrodevice	commercial	AEC	83.9°	1600	0.14	N/A	>400	0.3	>100	<0.01
	El-Kady et al. ¹¹	LSG	<20°	30	N/A	N/A	10	3.67 4.82	<10 20	<0.1 1.36
	Miller et al. ¹⁴	VG	82°	15000	~0.2	N/A	N/A	<0.2 N/A	N/A	N/A
	Sheng et al. ¹⁵	ErGO	85.5°	4200	1.35	0.24	350	<1 N/A	N/A	N/A
	Du and Pan ²³	CNTs	<75°	636	NA	1.5	1	N/A	N/A	N/A

^aG/CNTCs: graphene/carbon nanotube carpets; OLC: onion-like carbon; LRG: laser reduced graphene; AC: activated carbon; AEC: aluminum electrolytic capacitor; LSG: laser-scribed graphene; VG: vertical graphene; ErGO: electrochemical reduced graphene oxide; CNTs: carbon nanotubes. The cells in bold indicate an aqueous electrolyte; the cells in italics indicate an organic electrolyte. All of the data were based on the best result from each reference. ^bThe values are estimated from the given impedance Nyquist plots in the references.

The main reason why supercapacitors outperform conventional electrolytic capacitors is their porous nature. However, the confinement of ion flow due to this porous nature generally results in a poor ac response, which can be noted from the 45° line intersecting the real axis in their Nyquist plots.²⁴ Figure 2b shows representative Nyquist plots from microdevices constructed with CNTCs grown for 1, 2.5, and 5 min, with the inset showing an expanded view at the high-frequency region. The absence of a 45° line intersecting the real axis implies no features of a porous nature on the electrodes from the inset of the Figure 2b.¹⁴ The Nyquist plot for the supercapacitors usually shows a high-frequency semicircle caused by an effective series resistance,¹⁴ which is attributed to the ionic conductivity at the electrode–electrolyte interface.²⁵ Here, the absence of the semicircle in the Nyquist plots implies an ultrahigh ionic conductivity at the interface of the electrodes and electrolyte,¹⁵ consistent with the ultrahigh rate capability and high-power performance.²⁴ From the Nyquist plots, the series RC model was employed to estimate the specific areal capacitance (C_A) using equations described in Supplemental eq S1. The evolutions of C_A of microdevices prepared with CNTCs grown for 1, 2.5, and 5 min are plotted as functions of frequency in Figure 2c. All of the microdevices show capacitive behaviors at up to 10^4 Hz (Figure 2c). At 120 Hz, C_A are 230 $\mu\text{F}/\text{cm}^2$ for 1 min growth, 470 $\mu\text{F}/\text{cm}^2$ for 2.5 min growth, and 662 $\mu\text{F}/\text{cm}^2$ for 5 min growth. These are some of the highest capacitances reported to date in supercapacitors that are demonstrated to have ac line filtering performance.^{14,15} The measured total resistances of 21.3, 17.3, and 15.2 Ω at 120 Hz yield the RC time constants (τ_{RC}) of 195, 325, and 402 μs , respectively. These τ_{RC} values are comparable to AECs or vertical graphene DLC (VG-DLC, 200 μs),¹⁴ shorter than electrochemically reduced graphene DLC (ErG-DLC, 1.35 ms),¹⁵ and much shorter than 8.3 ms period required for 120 Hz filtering.^{14,15}

The real and imaginary capacitances, extracted from the impedance data, are important indicators of the performance of supercapacitors.²⁶ Figure 2d presents the evolution of specific real (C') and imaginary (C'') capacitances versus the frequency

(calculated in Supporting eqs S2 and S3). C' of all of the microdevices tend to be comparatively frequency-independent until 120 Hz, suggesting excellent capacitive behavior.²⁶ From the maximum frequency (f_0) of imaginary capacitance C'' , we can derive the characteristic relaxation time constant τ_0 ($= 1/f_0$) which is the minimum time for discharging all of the energy with an efficiency >50%.⁸ The extra small τ_0 (0.82 ms) for the microdevice with CNTCs grown for 1 min further confirms the ultrafast ion absorption/desorption. As the growth duration increases, τ_0 increases (1.78 ms for 2.5 min growth and 2.62 ms for 5 min growth) arising from the elongation of the ion diffusion path. Nevertheless, these values are much smaller than AC-MCs (700 ms)⁸ and OLC-MCs (26 ms).⁸ Such short τ_0 would enable G/CNTCs-MCs to deliver ultrahigh power density. In summary, to our knowledge, all of the above-discussed ac performance characteristics (impedance phase angles at 120 Hz, frequencies at phase angle of -45° , τ_{RC} , τ_0) are superior to past microdevices. The comparisons of various capacitors are summarized in Table 1.

In general, supercapacitors are used to deliver energy or power operated at only a few tens of Hertz. Thus, investigation of the power performance of the fabricated G/CNTCs-MCs is essential. Rate capability is an effective parameter to evaluate the power performance of supercapacitors, which can be obtained from cyclic voltammetry (CV) curves. Figure 3a–f exhibits CV curves at various scan rates from 0.1 to 500 V/s obtained in a microdevice constructed with CNTCs grown for 2.5 min using an aqueous electrolyte of 1 M Na₂SO₄. Compared to the microdevice with bare Ni contacts and graphene only, the microdevice constructed with added CNTCs exhibits significantly improved electrochemical performance, implying that the capacitance is mainly attributed to the ion absorption/desorption into the CNTCs, as expected (Figure 3a). The CV curves maintain near-ideal rectangular shapes with symmetric charge and discharge current densities at a scan rate of up to 100 V/s (Figure 3a–d), suggesting near-perfect formation of electrical double layer.²⁷ This is confirmed by the nearly triangular charge/discharge (CC) curves obtained at current densities from 0.1 to 100 mA/cm² (Supporting

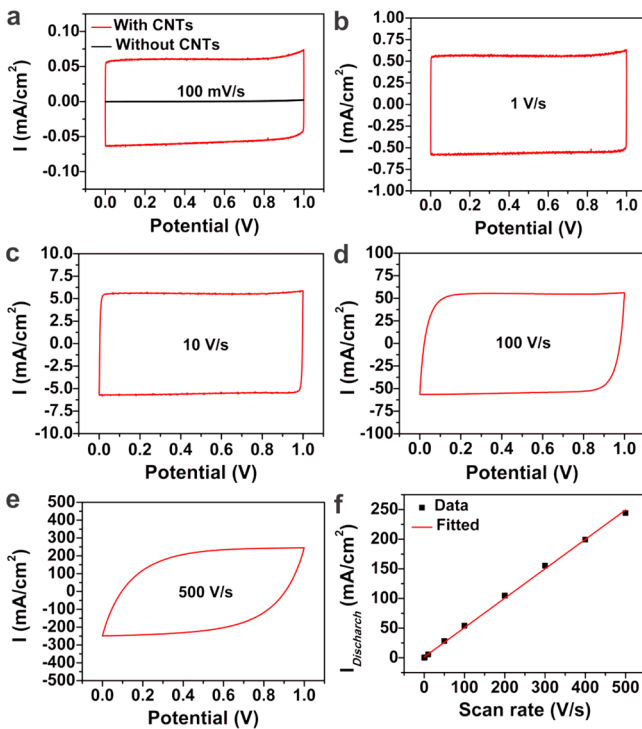


Figure 3. CV characterizations of G/CNTCs-MCs with CNTCs grown for 2.5 min and using 1 M Na_2SO_4 as the electrolyte. (a) CVs of microsupercapacitors with and without CNTCs obtained at a scan rate of 100 mV/s; (b–e) CVs obtained at various scan rates of 1, 10, 100, and 500 V/s; (f) discharge current densities as a function of scan rate.

Figure S3a,b). Although the transient effect of rounded corners is becoming obvious as the scan rate increases up to 400 V/s (Supporting Figure S3c,d), the specific capacitance, derived from the symmetric and constant steady-state current density, is still maintained.²⁸ The quasi-rectangular shape with little variance even at the ultrahigh scan rate of 500 V/s is noteworthy (Figure 3e). The evolved discharge current densities exhibit linear dependence scan rates from 0.1 to 400 V/s (Figure 3f), which is higher than the recent record in Er-DLC (350 V/s),¹⁵ much higher than OLC-MCs (100 V/s)⁸ or LSG-DLC (10 V/s),¹¹ and hundreds of times higher than the those from AC-MCs (1 V/s).¹⁰ This ultrahigh rate capability underscores the enhanced power performance of G/CNTCs-MCs. To further characterize the electrochemical performance of the microdevices, self-discharge measurements were performed. The open-circuit potential versus time is presented in Supporting Figure S4. In 6 h the potential shows a retention of $\sim 86\%$. The decay rate is calculated to be $\sim 6.8 \mu\text{V/s}$, which is among the best values ever reported for microsupercapacitors.⁹

Interestingly, we found that high-temperature water etching could significantly improve the capacitance of the fabricated microdevices. This is achieved by exposing the G/CNTCs-MCs to hydrogen and water vapor at 750 °C for 2 min. Figure S5a shows the CV curves of the representative microdevices with and without water etching. C_A increases by 103% from 0.70 mF/cm² to 1.42 mF/cm² after water etching (Supporting Figure S5a and calculated in Supporting eq S4). This enhancement might be due to two reasons: first, water could behave as the etching agent of amorphous carbon deposited on the surface of CNTs during their growth.²⁹ This would lower the effective series resistance between the electrolyte and CNTs in the RC model. Second, the water could attack the defect sites

of the CNTs to produce oxygen or hydroxyl functional groups,³⁰ which would improve the wettability of the CNTs and thus decrease the interfacial resistance. With the increased capacitance by water etching, the frequency at a phase angle of -45° decreases from 460 to 320 Hz (Supporting Figure S5b). If these frequencies are reversely proportional to the effective resistance times capacitance, the effective resistance after water etching decreases by 30%. In general, C_A calculated from CC curves using Supporting eq S5, increases as the growth duration is elongated (Supporting Figure S5c). Moreover, the water etching further enhances C_A by 50–110% (Supporting Figure S5c). This water treatment provides further capability of G/CNTCs-MCs to offer high power and energy density and strongly suggests that it is the residual effective series resistance of the electrolyte interface that limits high-frequency performance.

We also examined the electrochemical performance of the fabricated microdevices in an organic electrolyte. The micro-device was fabricated using 5 min growth CNTCs followed by postwater-etching for 2 min. 1-Butyl-3-methylimidazolium tetrafluoroborate (BMIM-BF₄) was used as the organic electrolyte. The galvanostatic CC curve in Supporting Figure S6a exhibits a nearly triangular shape, implying excellent double layer capacitive behaviors. Additionally, the cyclability test shows that the capacitance was retained at 98.4% even after 8000 cycles (Supporting Figure S6b). From the CC curves in Supporting Figure S7, we can further assess the electrochemical performance of G/CNTCs-MCs in terms of their specific capacitances, power densities, and energy densities. Figure 4a

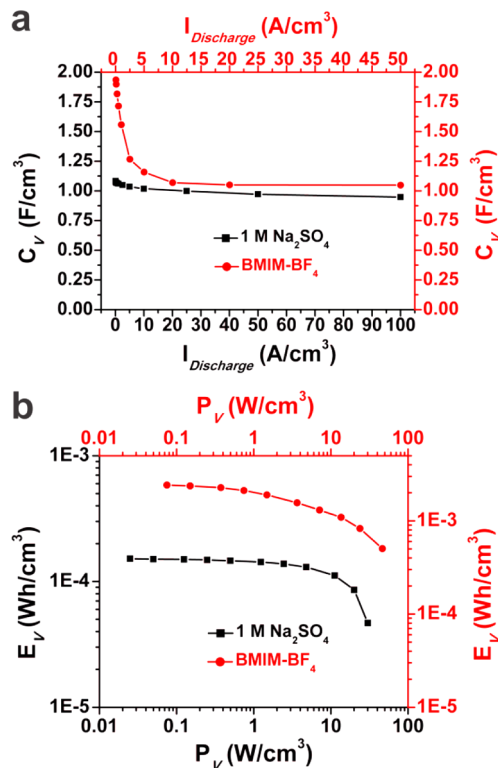


Figure 4. Comparison of electrochemical performance of G/CNTCs-MCs with CNTCs grown for 5 min followed by water etching for 2 min and using 1 M Na_2SO_4 and BMIM-BF₄ as electrolytes. (a) Comparison of C_V versus discharge volumetric current densities; (b) comparison, in the Ragone plots, of specific volumetric power density (P_V) and energy density (E_V).

exhibits the comparison of specific volumetric capacitance (C_V) of the microdevices made by the same growth conditions (CNTCs grown for 5 and 2 min water etching). The microdevices using 1 M Na_2SO_4 afford a C_V of 1.08 F/cm³_{volume} (or $C_A = 2.16 \text{ mF/cm}^2$), and this is decreased by 12% to 0.9 F/cm³_{volume} (or $C_A = 1.90 \text{ mF/cm}^2$) at an ultrahigh current density of 100 A/cm³_{volume} (or 200 mA/cm²), indicating the excellent rate capability. The microdevices using BMIM-BF₄ exhibit a C_V up to 1.96 F/cm³_{volume} (or $C_A = 3.93 \text{ mF/cm}^2$) and retain 1.05 F/cm³_{volume} (or $C_A = 2.10 \text{ mF/cm}^2$) at the ultrahigh current density of 50 A/cm³_{volume} (or 100 mA/cm²). When compared to the microdevices using Na_2SO_4 , the devices using BMIM-BF₄ show a relatively higher degradation because of the much larger ionic size than that of Na_2SO_4 . Nevertheless, the devices using BMIM-BF₄ still exhibit higher retention, even at much higher stack current density, than LSG-DLCs which degrades from 4.82 to 2.07 mF/cm² at a current density <10 A/cm³_{volume}.¹¹

A Ragone plot of a G/CNTCs-MC's energy density versus power density presents the device's operational range and provides information for optimizing the working point. The Ragone plots in Figure 4b show the performance comparison of microdevices using 1 M Na_2SO_4 and 1 M BMIM-BF₄ as the electrolytes. The specific volumetric energy (E_V) and volumetric power density (P_V) were derived from CC curves (Supporting Figure S7) by using Supporting eqs S6 and S7. The microdevices using BMIM-BF₄ exhibited much higher E_V (2.42 mWh/cm³) than the devices using Na_2SO_4 (0.16 mWh/cm³), mainly resulting from the wider operation potential window of 3 V in BMIM-BF₄. It should be noted that the E_V values, compared individually with the devices either using aqueous or organic electrolytes, are higher than LSG-DLC¹¹ or OLC-MCs,⁸ and more than 2 orders of magnitude higher than AECs.⁸ In addition, the G/CNTCs-MCs deliver P_V of 30 W/cm³ in aqueous electrolyte and 46 W/cm³ in BMIM-BF₄, which are comparable to OLC-MCs,⁸ higher than LRG-MCs⁹ or LSG-DLC.¹¹ The theoretical maximum P_V , obtained from Supporting eq S8, is as high as 115 W/cm³ in Na_2SO_4 and 135 W/cm³ in BMIM-BF₄, which are comparable to AECs or OLC-MCs.⁸ The detailed comparisons are summarized in Table 1.

In summary, we have developed microsupercapacitors based on 3D G/CNTCs hybrid materials with excellent electrochemical performance. The microdevices constructed with short CNTCs exhibit a much higher energy capacity than AECs while having comparable ac line filtering performances. With the increased heights of CNTCs, the as-produced microdevices show improved capacitances while maintaining satisfactory ac response. The most dramatic materials difference between these and other related structures are that the G/CNTCs have a seamless transition structure, maximizing the electrical conductivity. Water-etching significantly enhances the capacitance, resulting in ultrahigh power and energy densities. Given these performance characteristics, the G/CNTCs-MCs would provide a route to addressing the demands of the future microscale energy storage devices.

ASSOCIATED CONTENT

Supporting Information

Experimental, material characterizations, device characterizations, and additional figures. This material is available free of charge via the Internet at <http://pubs.acs.org>.

AUTHOR INFORMATION

Corresponding Author

*E-mail: natelson@rice.edu; tour@rice.edu.

Notes

The authors declare no competing financial interest.

ACKNOWLEDGMENTS

Funding for this research was provided by Boeing, the AFOSR MURI (FA9550-12-1-0035), Sandia National Laboratory (1100745), the Lockheed Martin Corporation through the LANCER IV Program, and the ONR MURI program (Nos. 00006766, N00014-09-1-1066).

REFERENCES

- (1) Miller, J. R.; Simon, P. *Science* **2008**, *321*, 651–652.
- (2) Simon, P.; Gogotsi, Y. *Nat. Mater.* **2008**, *7*, 845–854.
- (3) Pushparaj, V. L.; Shajumon, M. M.; Kumar, A.; Murugesan, S.; Ci, L.; Vajtai, R.; Linhardt, R. J.; Nalamasu, O.; Ajayan, P. M. *Proc. Natl. Acad. Sci.* **2007**, *104*, 13574–13577.
- (4) Hu, L. B.; Choi, J. W.; Yang, Y.; Jeong, S.; La Mantia, F.; Cui, L. F.; Cui, Y. *Proc. Natl. Acad. Sci.* **2009**, *106*, 21490–21494.
- (5) Zhu, Y. W.; Murali, S.; Stoller, M. D.; Ganesh, K. J.; Cai, W. W.; Ferreira, P. J.; Pirkle, A.; Wallace, R. M.; Cychoz, K. A.; Thommes, M.; Su, D.; Stach, E. A.; Ruoff, R. S. *Science* **2011**, *332*, 1537–1541.
- (6) Rolison, D. R.; Long, R. W.; Lytle, J. C.; Fischer, A. E.; Rhodes, C. P.; McEvoy, T. M.; Bourga, M. E.; Lubers, A. M. *Chem. Soc. Rev.* **2009**, *38*, 226–252.
- (7) Chmiola, J.; Largeot, C.; Taberna, P. L.; Simon, P.; Gogotsi, Y. *Science* **2010**, *328*, 480–483.
- (8) Pech, D.; Brunet, M.; Durou, H.; Huang, P. H.; Mochalin, V.; Gogotsi, Y.; Taberna, P. L.; Simon, P. *Nat. Nanotechnol.* **2010**, *5*, 651–654.
- (9) Gao, W.; Singh, N.; Song, L.; Liu, Z.; Reddy, A. L. M.; Ci, L. J.; Vajtai, R.; Zhang, Q.; Wei, B. Q.; Ajayan, P. M. *Nat. Nanotechnol.* **2011**, *6*, 496–500.
- (10) Pech, D.; Brunet, M.; Taberna, P. L.; Simon, P.; Fabre, N.; Mesnilgrente, F.; Conedera, V.; Durou, H. *J. Power Sources* **2010**, *195*, 1266–1269.
- (11) El-Kady, M. F.; Strong, V.; Dubin, S.; Kaner, R. B. *Science* **2012**, *335*, 1326–1330.
- (12) Liu, C. C.; Tsai, D. S.; Chung, W. H.; Li, K. W.; Lee, K. Y.; Huang, Y. S. *J. Power Sources* **2011**, *196*, 5761–5768.
- (13) Chen, C. H.; Tsai, D. S.; Chung, W. H.; Lee, K. Y.; Chen, Y. M.; Huang, Y. S. *J. Power Sources* **2012**, *205*, 510–515.
- (14) Miller, J. R.; Outlaw, R. A.; Holloway, B. C. *Science* **2010**, *329*, 1637–1639.
- (15) Sheng, K. X.; Sun, Y. Q.; Li, C.; Yuan, W. J.; Shi, G. Q. *Sci. Rep.* **2012**, *2*.
- (16) Futaba, D. N.; Hata, K.; Yamada, T.; Hiraoka, T.; Hayamizu, Y.; Kakudate, Y.; Tanaike, O.; Hatori, H.; Yumura, M.; Iijima, S. *Nat. Mater.* **2006**, *5*, 987–994.
- (17) Honda, Y.; Haramoto, T.; Takeshige, M.; Shiozaki, H.; Kitamura, T.; Ishikawa, M. *Electrochim. Solid-State Lett.* **2007**, *10*, A106–A110.
- (18) Paul, R. K.; Ghazinejad, M.; Penchev, M.; Lin, J.; Ozkan, M.; Ozkan, C. S. *Small* **2010**, *6*, 2309–2313.
- (19) Fan, Z. J.; Yan, J.; Zhi, L. J.; Zhang, Q.; Wei, T.; Feng, J.; Zhang, M. L.; Qian, W. Z.; Wei, F. *Adv. Mater.* **2010**, *22*, 3723–3728.
- (20) Zhu, Y.; Li, L.; Zhang, C.; Casillas, G.; Sun, Z.; Yan, Z.; Ruan, G.; Peng, Z.; Raji, O. A.-R.; Kittrell, C.; Hauge, H. R.; Tour, M. J. *Nat. Commun.* **2012**, DOI: 10.1038/ncomms2234.
- (21) Sun, Z.; Yan, Z.; Yao, J.; Beitler, E.; Zhu, Y.; Tour, J. M. *Nature* **2010**, *468*, 549–552.
- (22) Pint, C. L.; Alvarez, N. T.; Hauge, R. H. *Nano Res.* **2009**, *2*, 526–534.
- (23) Du, C. S.; Pan, N. *J. Power Sources* **2006**, *160*, 1487–1494.
- (24) Du, C. S.; Pan, N. *Nanotechnology* **2006**, *17*, 5314–5318.

- (25) Gamby, J.; Taberna, P. L.; Simon, P.; Fauvarque, J. F.; Chesneau, M. *J. Power Sources* **2001**, *101*, 109–116.
- (26) Taberna, P. L.; Simon, P.; Fauvarque, J. F. *J. Electrochem. Soc.* **2003**, *150*, A292–A300.
- (27) Pell, W. G.; Conway, B. E. *J. Electroanal. Chem.* **2001**, *500*, 121–133.
- (28) Bazant, M. *Electrochemical Energy Systems*; MIT: Cambridge, MA, 2011; Lecture 36: Electrochemical Supercapacitors.
- (29) Futaba, D. N.; Hata, K.; Yamada, T.; Mizuno, K.; Yumura, M.; Iijima, S. *Phys. Rev. Lett.* **2005**, *95*.
- (30) Amama, P. B.; Pint, C. L.; McJilton, L.; Kim, S. M.; Stach, E. A.; Murray, P. T.; Hauge, R. H.; Maruyama, B. *Nano Lett.* **2009**, *9*, 44–49.